

Preparation and characterization of flexible and thermally stable CuO nanocrystal-decorated SiO₂ nanofibers

Zhongliang Hu¹ · Zhijun Ma¹ · Xin He¹ · Chenxing Liao¹ · Yang Li¹ · Jianrong Qiu¹

Received: 26 April 2015 / Accepted: 2 July 2015 / Published online: 11 July 2015
© Springer Science+Business Media New York 2015

Abstract Nanofibers functionalized by semiconductor nanocrystals are drawing increasing interest, due to their widespread applications in the fields of new energy development, environment protection and chemical sensing, etc. Herein, we demonstrate a simple approach to prepare CuO/SiO₂ nanocomposite materials. The flexible SiO₂ nanofibers were prepared via the sol–gel electrospinning techniques. CuO nanocrystals were grafted on the surface of SiO₂ nanofibers by simply soaking and post-calcination. Micromorphology, structure and mechanical strength of SiO₂/CuO nanocomposite fibers were investigated by SEM, TEM and stress–strain test. Photocatalytic water purification ability of SiO₂/CuO nanofibers was evaluated by employing rhodamine B as a model pollutant. Our results indicated that the SiO₂/CuO nanofibers were flexible, thermally resistant and photocatalytic reactive, which promise the potential application in environmental remediation.

Keywords Electrospun SiO₂ nanofiber · CuO nanocrystals · Pechini sol–gel · Visible light photocatalysis

1 Introduction

Electrospinning-derived nanofibers functionalized with semiconductor nanocrystals have been a hot research topic these years, due to their features of continuously long shape and semiconducting nature [1–4]. Besides, nonwoven films with interconnecting nanoporous structure can be assembled by the nanofibers conveniently during the electrospinning process. Therefore, these kinds of materials are widely applied in many fields, including new energy development [5], environment protection [6, 7] and chemical sensing [8] etc. One-step preparation including electrospinning and post-calcination ensures the nanofibrous configuration of semiconductor nanofibers, but cannot give the acceptable mechanical strength, which limits their practical use. To address this issue, some efforts were devoted to polymer electrospun nanofibers, which were functionalized with semiconductor nanocrystals via post-surface modification. However, due to the big chemical discrepancy between the organic polymer and the inorganic semiconductor, to decorate semiconductor nanocrystals on the polymer nanofibers' surface still faces many challenges.

Copper oxide (CuO), an important p-type semiconductor with a band gap of 1.2–1.5 eV, has drawn a lot of research attention in recent years because of its widespread applications in catalysis, chemical sensing, magnetic storage, lithium batteries and solar cells [9–15], etc. So far, nanostructured CuO has been shown as an efficient photocatalyst for degradation of organic pollutants with visible light responsivity. CuO nanostructures with various morphologies, including microshuttles, porous microrods and straw sheaves etc., have been synthesized successfully [16–22]. Although the ultra-small CuO particles are highly reactive in photocatalysis, such size effect brings about

✉ Zhijun Ma
zhijma@scut.edu.cn

✉ Jianrong Qiu
qjr@scut.edu.cn

¹ State Key Laboratory of Luminescent Materials and Devices, School of Materials Science and Engineering, South China University of Technology, Guangzhou, China

many difficulties as the separation after photocatalytic reaction and their high surface energy also leads to easy agglomeration. Considering the manifold requirements of photocatalysts in practical use, the combination of photocatalyst with microfibrillar/nanofibrillar building blocks (typically electrospinning-derived nanofibers) to construct porous films is an effective scenario with high industrial feasibility [23, 24]. Up to now, both electrospinning-based fabrication of CuO nanofibers and electrospun ceramic nanofibers (e.g., TiO₂ and SnO₂) decorated with CuO nanoparticles have been reported [25–27]. Nevertheless, they lack enough manipulation convenience in practical use due to their brittleness.

In this work, we also make an attempt to combine CuO nanocrystals with electrospinning-derived nanofibers to construct composite nanofibrillar material through a very simple soaking–calcination approach. Different from previous works yet reported, here we employed inorganic but flexible electrospun SiO₂ nanofibers as the scaffold for supporting CuO nanoparticles. To provide an example of the practical application, photocatalytic water purification by the SiO₂/CuO nanofibers was performed using RhB as a model organic pollutant. With the advantages from both the SiO₂ nanofibers and the CuO nanoparticles, the composite SiO₂/CuO nanofibers simultaneously possess high flexibility, excellent thermal stability and high visible light photocatalytic reactivity, making it promising in environmental remediation.

2 Experimental section

2.1 Sample preparation

For preparation of the SiO₂ nanofibers, please refer to our previous work [28]. SiO₂–CuO composite nanofibers were synthesized through a Pechini sol–gel process. Cu(NO₃)₂ was dissolved in 20 mL water–ethanol (V:V = 1:7) solution containing citric acid as a chelating agent for the metal ions. The molar ratio of metal ions to citric acid was 1:2. As a cross-linking agent, polyethylene glycol (PEG, molecular weight = 10,000) was added with a final concentration of 0.2 g mL⁻¹. The solution was stirred for 2 h to form a transparent solution, and then, the SiO₂ nanofibers (in the form of nonwoven film) were soaked in the solution. After 8 h, the fibers were picked out and extraction-assisted filtrated to remove redundant soaking solution. And then the membrane was immediately dried at 100 °C for 1 h. Thoroughly dried samples were calcined at 500 °C in a muffle furnace for 2 h. For convenience, the final samples were nominated as SC. The concentration of Cu(NO₃)₂ was varied to investigate its influence on the morphology of the composite SC nanofibers (0.1, 0.25,

0.5 M, corresponding samples were denoted as SC-0.1, SC-0.25, SC-0.5, respectively).

2.2 Characterization

Micromorphology of the samples was characterized by a field-emission scanning electron microscopy (FE-SEM; ZEISS Merlin) and a transmission electron microscopy (TEM, JEOL-2100F). Crystalline structure of the samples was investigated by X-ray diffraction (XRD, Bruker AXS D8 Advance) using Cu K_α radiation ($\lambda = 0.154$ nm) as the source power. The mechanical property of the samples was measured with a tensile compression testing machine (USA, INSTRON5565).

2.3 Water purification performance

Photocatalytic water purification performance of SC nanofibers was evaluated with visible light illumination, using hydrogen peroxide (H₂O₂) as an oxidizer. A solar-500 Xe lamp (500W, Beijing NBeT Group Co. Ltd., China) with a 420-nm cut-off filter was used as the visible light source. The illumination spectrum normalized to 470 nm of simulated solar irradiation is presented in Fig. 1b RhB, (Chemical pure, Sinopharm) was adopted as a model organic pollutant. In the first test, nonwoven film of SC was attached at the bottom of a double-layer water-cooled glass beaker containing 20 mL RhB solution with the concentration of 60 mg L⁻¹, and then 0.2 mL H₂O₂ solution (30 % v/v) was added into the RhB solution to trigger the photocatalytic reaction. For comparison, the tests with H₂O₂ but without visible light irradiation, and with visible light irradiation but without the addition of H₂O₂ were also performed. In the second set of investigation, the water purification by the SC film was carried out via simple filtration with the SC film as the filter on a homemade setup, as schematically illustrated by Fig. 1a. Briefly, the SC film (SC-0.25) was fixed at the bottom of a glass tube with two rubber rings; then, the RhB solution (20 mL, 60 mg L⁻¹) containing H₂O₂ (~ 0.17 mol L⁻¹) was continuously fed into the glass tube under visible light irradiation with a flow rate of 60 mL h⁻¹. The filtration of the same bath of RhB solution was repeated for several times to monitor the concentration variation as a function of filtration cycles. Every cycle, after all the 20 mL RhB solution was filtered, the RhB concentration was measured and recorded. To demonstrate the thermal stability and recovery ability of the samples, after the water purification test, the film was dried thoroughly and calcined in a muffle furnace at 500 °C for 2 h to remove the organic residue. The photocatalytic activity of the calcined film was investigated under the same condition as the pristine film. In detail, after the first run of photocatalytic decomposition of the RhB solution,

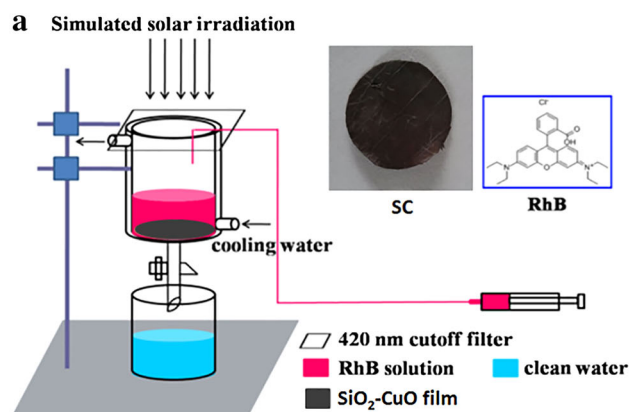
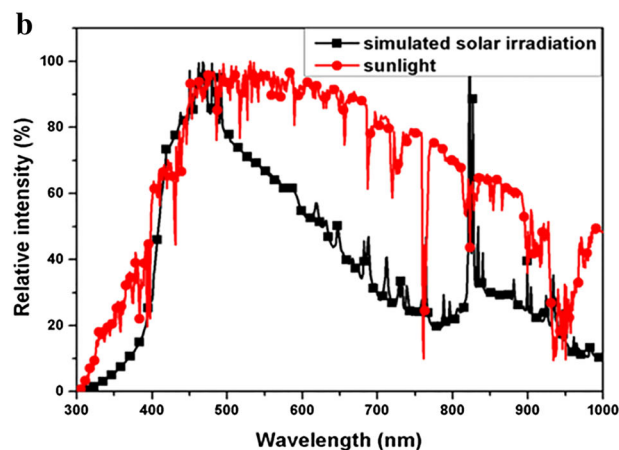


Fig. 1 **a** Schematic illustration of the homemade setup for evaluation of water purification performance of the composite SC films, the inset shows the molecular structure of RhB and the digital image of the SC

the film was picked out of the solution and dried thoroughly at 100 °C for 1 h, then transferred to a muffle furnace and calcined at 500 °C for 2 h. The above drying–calcination–photocatalysis process was repeated for three cycles. Photocatalytic behavior of the same sample without bending and bending for 10 and 20 times was tested. Concentrations of the RhB solutions before and after filtration were measured with a UV–Vis–IR spectrophotometer (Perkin Elmer Lambda 900, Waltham, MA).

3 Results and discussion

As shown by the SEM image in Fig. 2a, the electrospun SiO₂ nanofibers are continuous. Their average diameter was measured to be about 300 nm. A statistical diameter-distribution histogram is illustrated in Fig. 2b. The XRD pattern of electrospun SiO₂ fibers is shown in Fig. 2c. There is only one broadened envelope centering at around $2\theta = 22^\circ$, which should be assigned to the amorphous SiO₂ [JCPDS-29-0085] [29]. The mechanical property of the nonwoven film composed of SiO₂ fibers was tested, as shown in Fig. 2d. The tensile stress–strain curve indicates that the breakage of the film happened when the tensile stress increased to 1 MPa, and the tension strain reached to 0.012 mm mm⁻¹. It shows the breakage of the film was a relatively mild process rather than an abrupt tear, which should be ascribed to the interconnecting effect of the ultra-small fibers. The digital image of the tailored SiO₂ film in flat (d_1) and curled (d_2) status are shown in the inset of Fig. 2d, indicative of acceptable flexibility of the fibers. The flexibility of the silica mats was a result of the very small size of the nanofibers (average diameter about 300 nm). Small size of the materials led to an increase



film (SC-0.25); **b** the illumination spectrum normalized to 470 nm of simulated solar irradiation

volume percentage of the boundary component and decreased of the stress concentration, which reduce the chance of the generation and extension of the microcracks on the fibers [30].

Decoration of SiO₂ fibers with CuO nanoparticles was realized via a simple Pechini sol–gel process combined with post-calcination. Figure 3a, b shows the SEM and TEM images of SC-0.25 fibers. Very small nanoparticles of CuO with approximately bead-like shape that stick over the surface of SiO₂ fibers can be clearly observed. The mean size of the CuO nanobeads was calculated to be ~80 nm by measuring 100 pieces of particles. Figure 3c presents the high-resolution TEM image of a CuO nanoparticle on the fiber's surface. The distinct lattice fringe ensures the good crystallinity of CuO nanoparticles. The fringes with the inter-plane distances of 0.23, 0.25 and 0.27 nm correspond to (111), (-111) and (110) crystalline planes of the mono-clinic-phase CuO crystals. From the fringes pattern, it can be discerned that the CuO nanoparticle is composed of multiple monocrystals. The SAED (selected area electron diffraction) image of the CuO nanoparticle is displayed in Fig. 3d. From the disordered pattern of the dots lattice, the polycrystalline nature of the CuO nanoparticles can also be determined. Influence from the precursor Cu(NO₃)₃ concentration on the morphology and structure of the SC fibers was also investigated. As shown in Fig. 4a–c, with increasing the Cu²⁺ concentration in the precursor solution, both the population density and size of CuO nanoparticles on the fibers' surface increased obviously. For SC-0.1, besides the small particles on the fibers' surface, there are some relatively big agglomerations with the size in the scale of 1–3 μm at the connecting points of the fibers, as marked by the red arrows in Fig. 4a. At this moment, however, the origin mechanism of the big

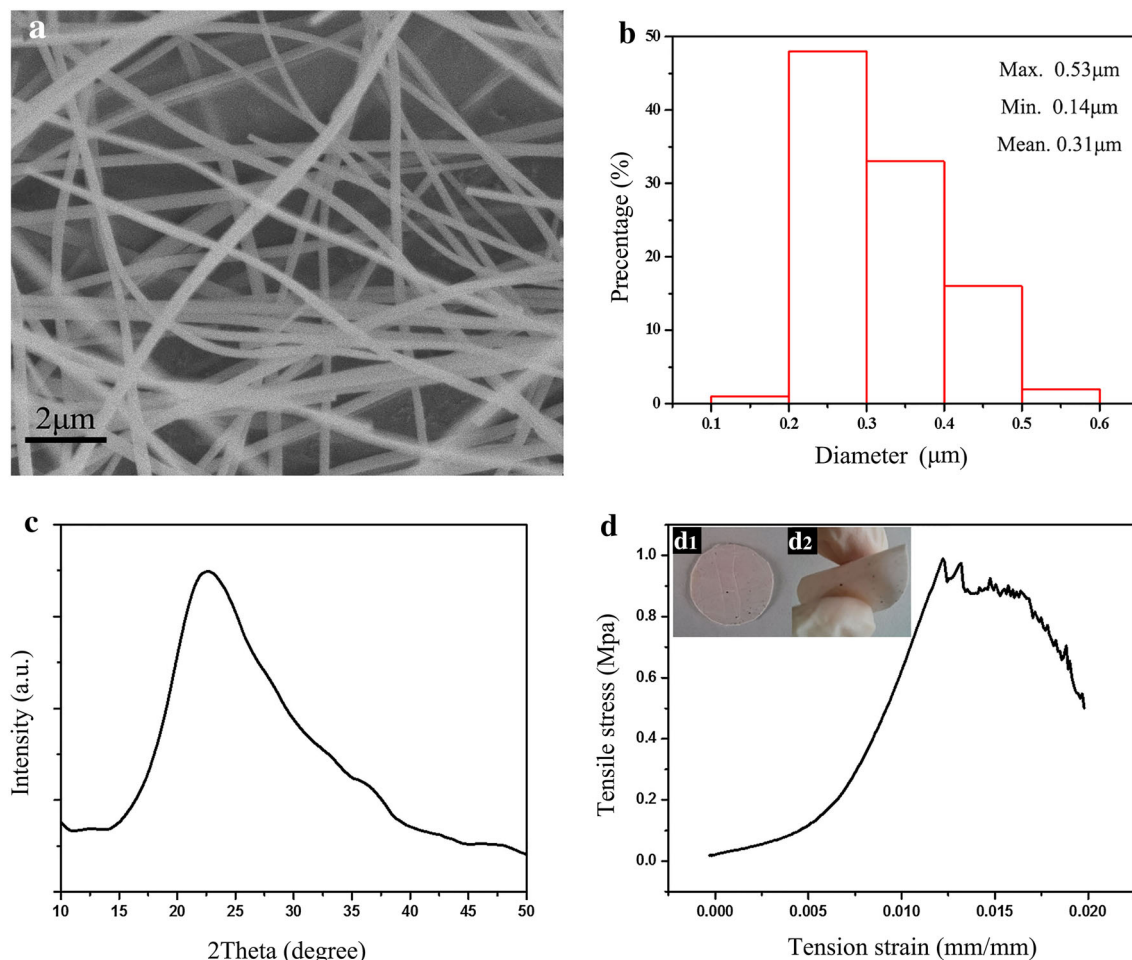


Fig. 2 **a** SEM image of the electrospun SiO_2 fibers; **b** statistical diameter distribution of the electrospun SiO_2 fibers; **c** XRD pattern of the electrospun SiO_2 fibers; **d** stress–strain curve of the SiO_2 fibrous film, the inset shows the digital images of the film in flat and curled status

agglomerations has not been clarified, more detailed study is required. For SC-0.25 and SC-0.5, such agglomerations cannot be observed. The mean size of the CuO nanoparticles of SC-0.1 (not including the big agglomerations), SC-0.25 and SC-0.5 was measured to be 40, 80 and 140 nm, respectively. For sample SC-0.5, parts of the CuO nanoparticles even interconnected together, forming CuO film spanning across the voids among SiO_2 fibers, as marked by the red circle in Fig. 4c. We assume that such porous CuO film-like structure would be beneficial to improve the photocatalysis performance of the SC film. High-magnification SEM images (the inset figures) present more detailed microstructures of the SC fibers. Figure 4d–f shows the EDS results which reveal that the mass ratios of CuO for SC-0.1, SC-0.25 and SC-0.5 are 34.9, 48.0 and 62.6 %, respectively, showing a monotonic increasing trend with the increase in the $\text{Cu}(\text{NO}_3)_2$ concentration. Figure 4g–i shows the EDS spectrum of SiO_2 films immersed in 0.25 M $\text{Cu}(\text{NO}_3)_2$ precursor solution with

different soaking time (ST). The result indicates that with increasing soaking time the CuO fraction did not change obviously, which means after achieving absorption equilibrium, the soaking time has little influence to the final products.

Figure 5a shows the XRD patterns of the samples. Besides the broad peak from amorphous SiO_2 at around 22.0° , other peaks at 32.5° , 35.7° , 38.9° , 49.0° , 53.7° , 58.3° , 61.8° , 66.6° , 68.1° are ascribed to the diffractions from (110), (002), (111), (-202), (020), (202), (113), (-311), (220) crystalline planes of mono-clinic CuO phase (JCPDS 49-0973). With the increase in $\text{Cu}(\text{NO}_3)_2$ concentration, the XRD peak intensity of the CuO nanocrystals increases monotonically, implying the increase in the mass ratio of CuO of the SC films, which agrees well with the SEM images in Fig. 4a–c. Figure 5b shows the stress–strain curves of samples SC-0.1, SC-0.25 and SC-0.5. When the concentration of Cu^{2+} was lower than 0.25 M, the breakage threshold of SC films was higher than that of

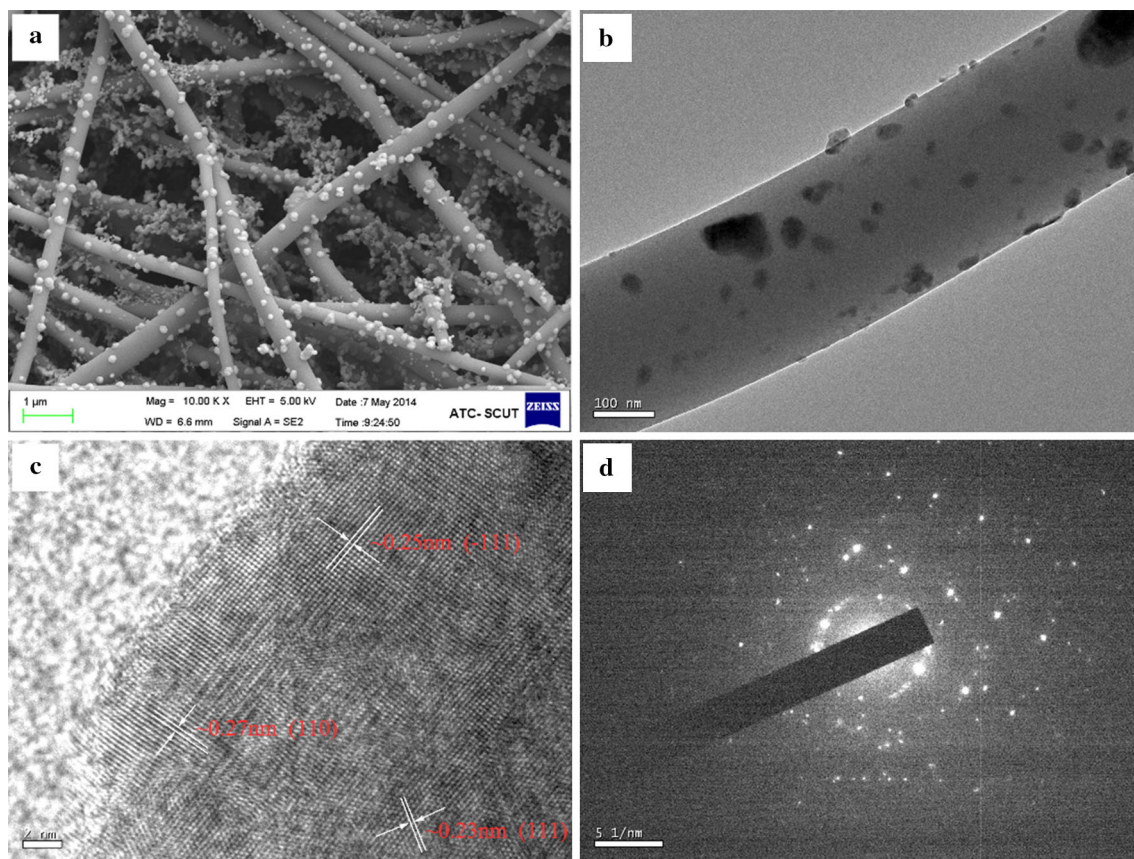


Fig. 3 **a** SEM image of SC-0.25; **b** TEM image of one single SC-0.25 fiber; **c** high-resolution TEM image of a CuO nanoparticle on the fiber's surface; **d** SAED image of a single CuO nanoparticle

the pristine SiO₂ nanofibrous film, which was 1.28 MPa and 1.07 MPa for SC-0.1 and SC-0.25, respectively. Both SC-0.1 and SC-0.25, especially SC-0.25, exhibited a mild and prolonged breaking process. While the concentration of Cu²⁺ further increased up to 0.5 M, the SC film became brittle and it presented a relatively abrupt breaking style. It is assumed that when the concentration of Cu(NO₃)₂ is relatively low, only very small CuO nanoparticles on the surface of the fibers and at the intervals between the fibers were grown, which formed a connecting network that strengthened the connection of SiO₂ fibers and in turn enhance the SC films' strength. When the concentration of Cu²⁺ is too high, more and bigger CuO particles were produced, which imposed too high stress on the SiO₂ fibers and made the SC film relatively crisp. Figure 5c shows the digital images of the SC-0.25 film in flattened and curled status. After being curled and then recovered, the film remained integral without serious damage. The mechanical strength of the SC films is acceptable in some practical use, for example water purification. Detailed data of mechanical properties of the samples are summarized in Table 1. Here N₂ adsorption–desorption test was employed to further

characterize the microstructure of the samples. As show in Fig. 5d, SiO₂ fibers and SC fibers both exhibited a type-IV N₂ adsorption–desorption isotherms with obvious hysteresis loops. Specific surface area and total pore volume of the SiO₂ fibers were calculated to be 12.02 m² g⁻¹ and 0.012 cc g⁻¹, respectively. The SC-0.25 film was more porous, its specific surface area and total pore volume increased to 55.59 m² g⁻¹ and 0.073 cc g⁻¹, respectively, while its average pore size was calculated to be 2.95 nm.

Photocatalytic water purification performance of the composite SC-0.25 fibers was evaluated by monitoring the degradation of RhB, in the presence of H₂O₂ as an oxidizing agent under visible light irradiation. The time dependence of the degradation of RhB solution is shown in Fig. 6a. The black, magenta red and blue lines correspond to the different experiment conditions described above. The RhB solution nearly maintained the same as its initial concentration in the presence of both SC-0.25 and H₂O₂ (the black line) but without light irradiation. The SC-0.25 exhibited weak photocatalytic reactivity under visible light irradiation but without the assistance

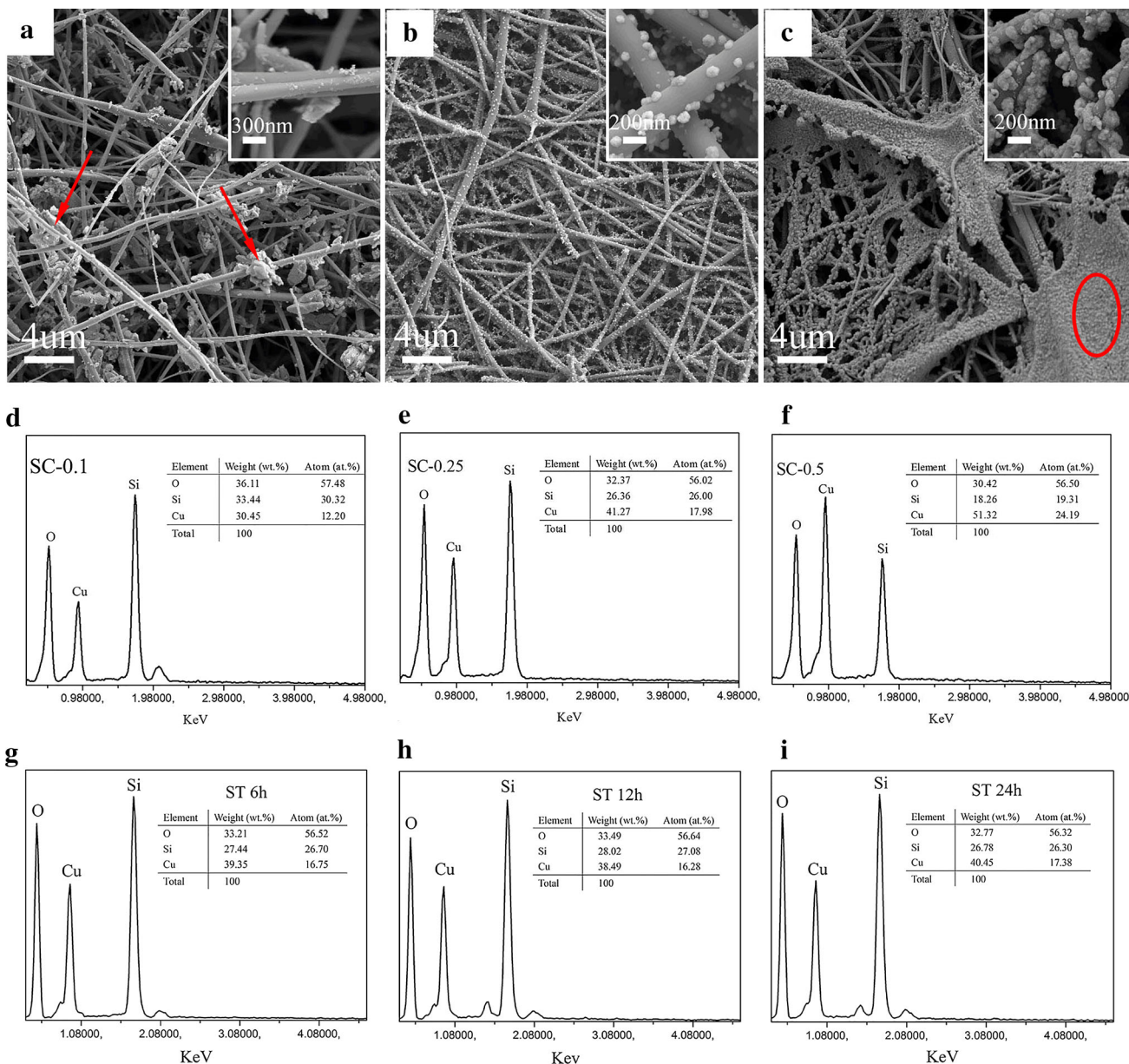


Fig. 4 SEM image of **a** SC-0.1, **b** SC-0.25, **c** SC-0.5. The corresponding insets show high-magnification SEM images of each sample. **d–e** the corresponding EDS spectra of sample SC-0.1, SC-0.25, SC-0.5, **g–i** the EDS spectra of SiO₂ films immersed in 0.25 M Cu(NO₃)₂ precursor with different soaking time

from H₂O₂ (the magenta line), and the corresponding decomposition rate of RhB was 4.8 mg g⁻¹ h⁻¹. H₂O₂ alone also presented certain degree of reactivity toward decomposing RhB with light irradiation, but the efficiency was as low as 1.2 mg mL⁻¹ h⁻¹ (the red line). With the simultaneous assistance from both light irradiation and trace concentration of H₂O₂, the SC-0.25 demonstrated remarkably enhanced photocatalytic reactivity, the corresponding decomposing efficiency of RhB substantially increased to 75 mg g⁻¹ h⁻¹ (the blue line). Figure 6b

shows the variation of the absorption spectrum of RhB aqueous solution in the presence of both the SC-0.25 and H₂O₂ at various time intervals, which is corresponding to the blue line in Fig. 6a. The characteristic absorption peaks of RhB molecules, attenuated gradually as the exposure time was prolonged, and nearly disappeared after 150 min of reaction. We further evaluated the water purification performance of SC films via simple filtration. Figure 6c shows the decomposition of RhB as a function of filtration cycles, with different samples as filter film

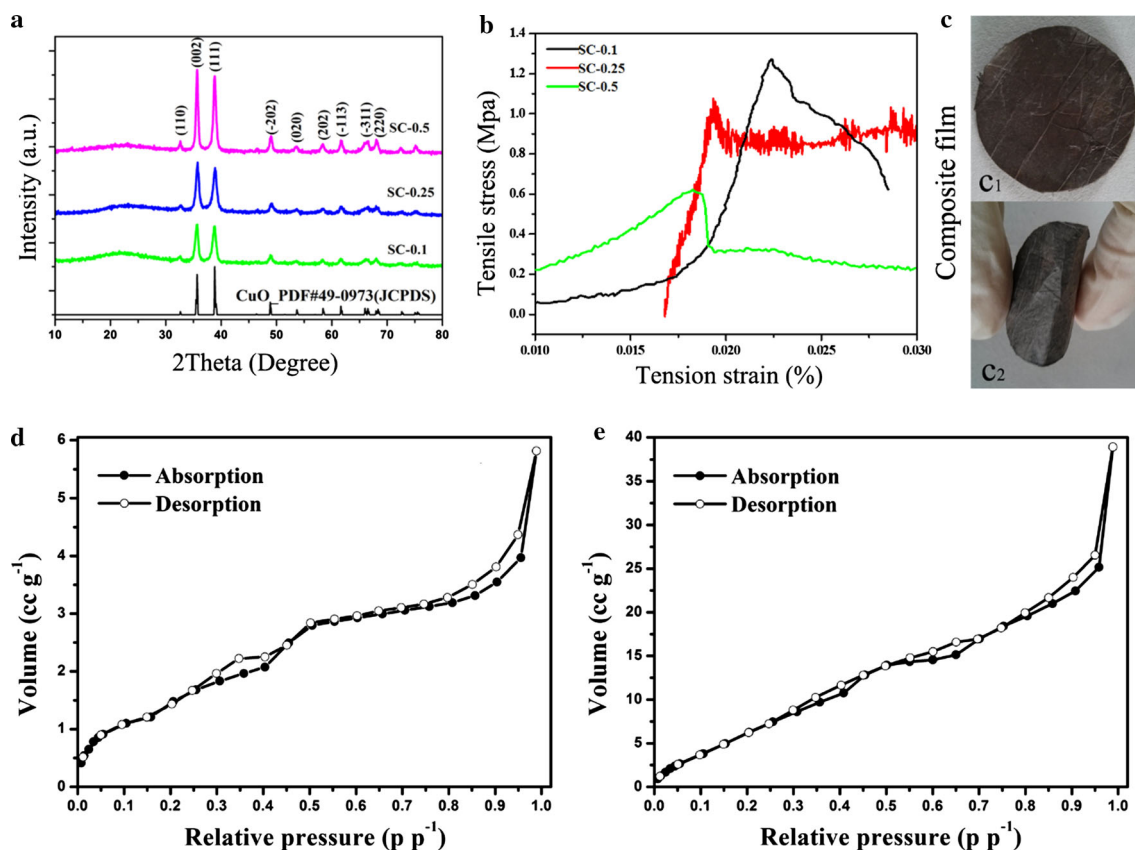


Fig. 5 **a** XRD spectra of samples SC-0.1, SC-0.25, SC-0.5; **b** strain–stress curves of samples SC-0.1, SC-0.25, SC-0.5; **c** digital pictures of the SC-0.25 film at flattened (c_1) and curled (c_2) status; **d**, **e** N_2 adsorption–desorption isotherms of SiO_2 fibers and SC-0.25 film

Table 1 Mechanical parameters calculated from stress–strain curves of SC-0.1, SC-0.25, SC-0.5 and SiO_2 film

Sample	Maximal load (N)	Tensile stress at maximal load (MPa)	Tensile strain at maximal load (%)	Elastic modulus (MPa)
SC-0.1	1.96	1.28	2.23	396.7
SC-0.25	1.53	1.07	1.93	220.3
SC-0.5	0.71	0.62	1.83	64.10
SiO_2 film	1.44	0.99	1.22	165.82

under visible light irradiation and in the presence of trace amount of H_2O_2 . After five cycles of filtration, the remaining RhB in the three sets of experiments was measured to be 6.1, 4.3 and 1.1 %, respectively, which indicates that all samples possess high photocatalytic reactivity. Figure 6d, corresponding to the red line in Fig. 6c (SC-0.25), shows the variation of the absorption spectrum of the RhB solution as a function of filtration cycles. The intensity attenuation of the absorption of RhB was accompanied by gradual blue shift of the major peak positioning at around 553 nm, stemming from the

stepwise de-ethylation of the RhB molecules. We further demonstrate the thermal stability of SC film. As shown in Fig. 7a, after three times of heat treatment, the SC-0.25 film maintained its photocatalytic reactivity very well, almost no performance degradation was observed, indicative of excellent thermal stability. Figure 7b shows the photocatalytic behavior of SC-0.25 film after bending the membrane for different times. The result indicates that even bending the membrane for 20 times (here BT represent bending times), the photocatalytic property of the sample remains the same as initial.

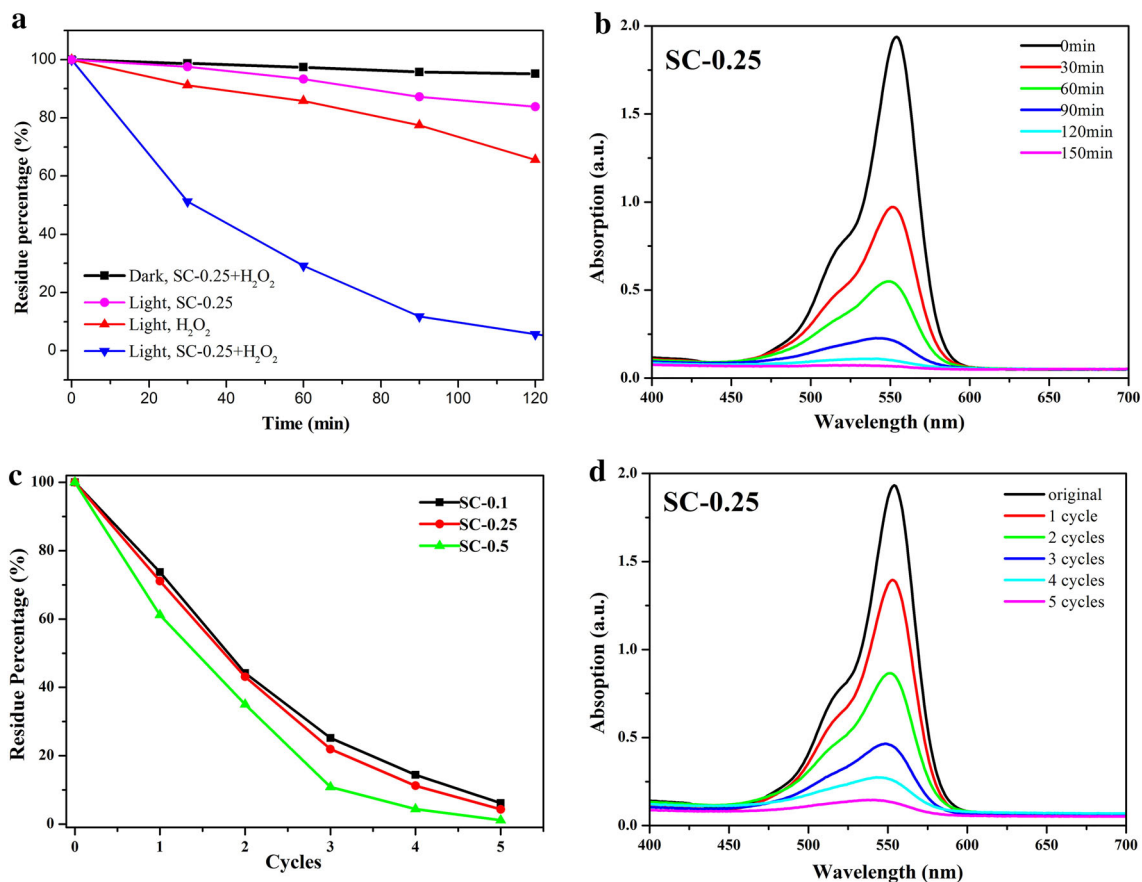


Fig. 6 **a** Degradation kinetics of RhB with SC-0.25 in different conditions; **b** variation of absorption spectrum of RhB aqueous solution in the presence of both the SC-0.25 and H₂O₂ at various time intervals; **c** photocatalytic decomposition of RhB via simple filtration

with the SC films as the filter; **d** variation of absorption spectra of RhB aqueous solution with SC-0.25 as the filter after different cycles of filtration

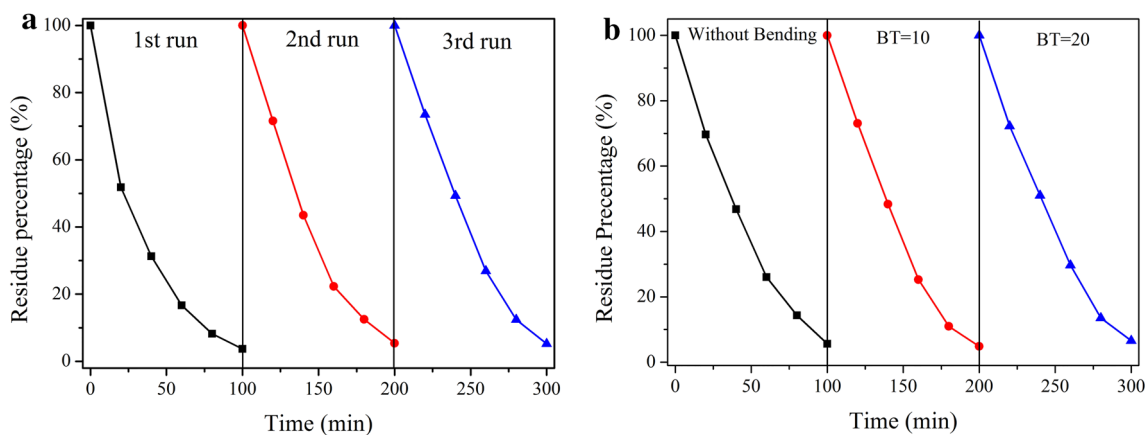


Fig. 7 **a** The degradation kinetics of RhB with SC-0.25 film as photocatalyst running for three cycles of recycling use. In each cycle, before the photocatalysis test, the film was dried and calcined at 500° for 2 h. **b** Photocatalytic behavior of SC-0.25 film without bending

(black line) and after bending the membrane for 10 times (red line) and 20 times (blue line). (BT inset of the figure means bending times) (Color figure online)

4 Conclusion

In summary, we propose a simple but efficient approach for preparation of CuO/SiO₂ (SC) nanofibers, by using the electrospinning technique and the Pechini sol–gel method. We employed H₂O₂ as the concentration indicator to show the remarkable photocatalytic ability of SC nanofibers under visible light irradiation. When the concentration of Cu(NO₃)₂ in the precursor solution was optimized, the SC fibers exhibited both acceptable mechanical strength and high photocatalytic reactivity, which is very useful in some practical applications. Due to the stabilization effect from the SiO₂ fibers, agglomeration of CuO nanoparticles can be readily avoided during the water purification process, being beneficial to keep the high photocatalytic activity of the SC fibers. Furthermore, the completely inorganic nature endows the SC fibers with excellent thermal resistance, which makes it possible to recover its photocatalytic reactivity after removal of organic pollutants by simple calcination. The approach employed here opens a new path to prepare other types of semiconductor nanocrystals functionalized fibrous materials using electrospun SiO₂ fibers as the scaffold, and more efforts are being conducted in our group. Further progress will be reported later.

Acknowledgments This work is financially supported by the National Natural Science Foundation of China (Grants Nos. 51132004, 51302087), and Fundamental Research Funds for the Central Universities (Grants No. 2014ZM0002).

References

- Wold A (1993) *Chem Mater* 5:280–283
- Zhang Z, Shao C, Li X, Sun Y, Zhang M, Mu J, Zhang P, Guo Z, Liu Y (2012) *Nanoscale* 5:606–618
- Zhang X, Li X, Shao C, Li J, Zhang M, Zhang P, Wang K, Lu N, Liu Y (2013) *J Hazard Mater* 260:892–900
- Zhang Y, Liu S, Xiu Z, Lu Q, Sun H, Liu G (2014) *J Nanopart Res* 16:2375
- Babu VJ, Kumar MK, Nair AS, Kheng TL, Allakhverdiev SI, Ramakrishna S (2012) *Int J Hydrog Energy* 37:8897–8904
- Kim CH, Kim B, Yang KS (2012) *Carbon* 50:2472–2481
- Sahay R, Kumar PS, Sridhar R, Sundaramurthy J, Venugopal J, Mhaisalkar SG, Ramakrishna S (2012) *J Mater Chem* 22:12953
- Han L, Andrady AL, Ensor DS (2013) *Sens Actuators B Chem* 186:52–55
- Bandara J, Udawatta CPK, Rajapakse CSK (2005) *Photochem Photobiol Sci* 4:857
- Yang C, Su X, Xiao F, Jian J, Wang J (2011) *Sens Actuators B Chem* 158:299–303
- Dar MA, Kim YS, Kim WB, Sohn JM, Shin HS (2008) *Appl Surf Sci* 254:7477–7481
- Gao XP, Bao JL, Pan GL, Zhu HY, Huang PX, Wu F, Song DY (2004) *J Phys Chem B* 108:5547–5551
- Wang H, Pan Q, Zhao J, Yin G, Zuo P (2007) *J Power Sources* 167:206–211
- Anandan S, Wen X, Yang S (2005) *Mater Chem Phys* 93:35–40
- Sahay R, Sundaramurthy J, Kumar PS, Thavasi V, Mhaisalkar SG, Ramakrishna S (2012) *J Solid State Chem* 186:261–267
- Chen Y, Tao X, Min Y, Zheng F (2013) *J Mater Sci Mater Electron* 24:1319–1324
- Huang J, Fu G, Shi C, Wang X, Zhai M, Gu C (2014) *J Phys Chem Solids* 75:1011–1016
- Li J, Sun F, Gu K, Wu T, Zhai W, Li W, Huang S (2011) *Appl Catal A Gen* 406:51–58
- Zhao Y, Shi H, Chen M, Teng F (2014) *Cryst Eng Commun* 16:2417
- Sathyamoorthy R, Mageshwari K (2013) *Physica E* 47:157–161
- Rabbani M, Rahimi R, Bozorgpour M, Shokraiyani J, Moghadam SS (2014) *Mater Lett* 119:39–42
- Umadevi M, Christy AJ (2013) *Spectrochim Acta A* 109:133–137
- Im JS, Kim MI, Lee Y (2008) *Mater Lett* 62:3652–3655
- Lee JA, Krogman KC, Ma M, Hill RM, Hammond PT, Rutledge GC (2009) *Adv Mater* 21:1252–1256
- Guan H, Shao C, Chen B, Gong J, Yang X (2003) *Inorg Chem Commun* 6:1409–1411
- Lee SS, Bai H, Liu Z, Sun DD (2013) *Water Res* 47:4059–4073
- Zhao Y, He X, Li J, Gao X, Jia J (2012) *Sens Actuators B Chem* 165:82–87
- Ma Z, Ji H, Teng Y, Dong G, Zhou J, Tan D, Qiu J (2011) *J Colloid Interface Sci* 358:547–553
- Wu JH, Li XS, Zhao Y, Gao Q, Guo L, Feng YQ (2010) *Chem Commun* 46:9031–9033
- Guo M, Ding B, Li XH, Wang XL, Yu JY, Wang MR (2010) *J Phys Chem C* 114:916–921